Russian Journal of Applied Chemistry, Vol. 77, No. 3, 2004, pp. 353–359. Translated from Zhurnal Prikladnoi Khimii, Vol. 77, No. 3, 2004, pp. 359–365.

INORGANIC SYNTHESIS AND INDUSTRIAL INORGANIC CHEMISTRY

Formation of the Structure of C–SiC–Si–Al Composites

E. A. Belenkov and E. M. Baitinger

Chelyabinsk State University, Chelyabinsk, Russia
Chelyabinsk State Pedagogical University, Chelyabinsk, Russia

Received January 29, 2002; in final form, December 2002

Abstract—Transmission electron microscopy and X-ray structural analysis were applied to study the fundamental aspects of formation of the crystal structure of C–SiC–Si–Al composites. The reasons why spatially heterogeneous regions are formed were revealed.

C–SiC composites are commonly obtained by reaction of porous carbon supports with molten silicon [1–3]. To modify the properties of such materials, metal impurities are added to the silicon melt. However, these additives frequently lead to appearance of spatial heterogeneities, which adversely affects the strength properties of composites [4]. This study is concerned with the structure of C–SiC–Si composites with admixture of aluminum.

EXPERIMENTAL

As objects of study were chosen the composites PG–AS, GP–0.5AS, and MG–AS [5], synthesized by reaction of PG-50, PROG-2400, and ARV porous carbon materials with an Si + Al melt. The content of aluminum in the melt was ~10 wt % in synthesizing the PG–AS and MG–AS composites and ~5 wt % in the case of GP–0.5AS. Selected properties and the composition of the composites and the carbon supports, taken from [3, 5], are listed in Table 1.

Samples for comparative X-ray studies were prepared in the form of 100 × 14 × 14-mm slabs. Samples for analysis of how the phase composition varies across the cross section of the MG–AS composite were obtained using a diamond saw in accordance with the scheme shown in Fig. 1.

The X-ray diffraction analysis was carried out with a DRON-3 diffractometer (CuK_α radiation with λ = 0.15418 nm). The phase analysis and indexing of X-ray diffraction patterns were performed using the ASTM file. The profiles of the diffraction peaks were measured at a scanning rate of 0.25 deg min^{-1}. The interplanar spacings d were calculated from the centers of gravity of the diffraction peaks [6]. The average size L of the coherent domains was determined from the integral width β of diffraction peaks [6], with silicon and silicon carbide used as references. The electron-microscopic studies were carried out with a PEM-100 electron microscope.

Typical electron diffraction patterns of C–SiC–Si–Al composites are shown in Fig. 2. An analysis of the

Table 1. Properties and compositions of the samples studied

Material	Support	Pore radius,* μm	Porosity,* cm^3 g^{-1}	Composition,** wt %				ρ**	ρ***
				C	Si	SiC	Al	g cm^{-3}	
PG-50	–	3.98–8.95	0.46–0.517	100	–	–	–	1.00	–
ARV	–	3.76–4.50	0.173–0.182	100	–	–	–	1.55	–
PROG-2400	–	4.42–7.33	0.10–0.147	100	–	–	–	1.65	–
PG–AS	PG-50	–	–	22–23	15	55	7–8	2.63	2.59
MG–AS	ARV	–	–	22–23	15	55	7–8	2.30	2.16
GP–0.5AS	PROG-2400	–	–	–	–	–	–	–	2.47

* Data of [5].
** Data of [3].
*** Determined in this work.

1070-4272/04/7703-0353 © 2004 MAIK "Nauka/Interperiodica"

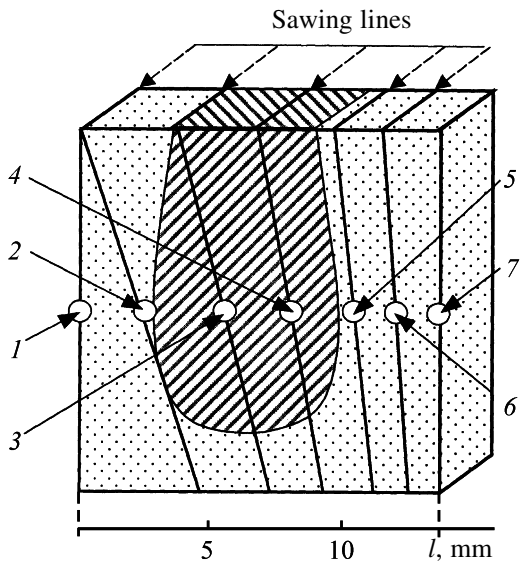

Fig. 1. Schematic of a study of how the phase composition and crystal structure varies across a sample of the MG–AS composite. (*1–7*) Region for which X-ray diffraction patterns were measured. (*l*) Distance; the same for Fig. 4.

electron diffraction patterns demonstrated that they can be related to microdiffraction from turbostratic carbon, silicon carbide, silicon, and aluminum. The probability of observing electron diffraction patterns of various phases widely varies across a sample. Regions that differ in contrast from the bulk of the material can be seen even visually on the edge cross sections of the GP–0.5AS and MG–AS composites. In Fig. 3, they are marked schematically with dark hatching and denoted by symbol C. Only electron diffraction patterns characteristic of carbon are recorded within these regions.

A comparative analysis performed for the MG–AS composite demonstrated that the crystal structure of carbon in the bulk of the composite is markedly different from the structure of carbon in C inclusions. Indeed, four basic types of electron diffraction patterns of turbostratic carbon are observed in the composites under study: (1) annular [characteristic of microscopic volumes occupied by crystals ~1 nm in size (Fig. 2a)], (2) annular with small number of discrete reflections [characteristic of a mixture of crystals ~1 and ~10 nm in size (Fig. 2b)], (3) discrete–ring-like [characteristic of microscopic volumes occupied by crystals ~10 nm in size (Fig. 2c)], and (4) discrete-periodic (characteristic of electron scattering by separate coarse crystals with size of ~100 nm and more (Fig. 2d)].

The probability of observing electron diffraction patterns of various types can be evaluated using the

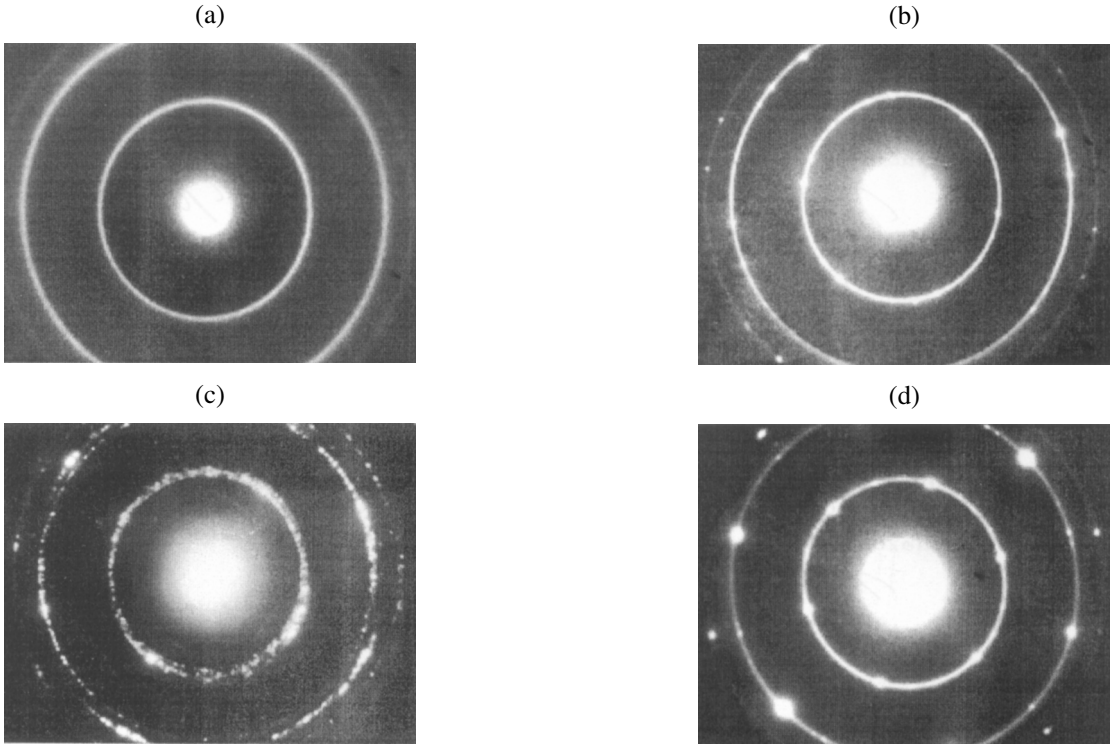

Fig. 2. Typical electron diffraction patterns of turbostratic carbon contained in C–SiC–Si–Al composites. Electron diffraction pattern: (a) ring-like, (b) ring-like with small number of discrete reflections, (c) discrete, and (d) discrete-periodic.

Table 2. Occurrence frequency of various types of electron diffraction patterns of turbostratic carbon in different regions of the MG–AS composite (Fig. 2)

Type of electron diffraction pattern	Bulk		Carbon inclusion C	
	number of electron diffraction patterns	%	number of electron diffraction patterns	%
1	8	8	44	41
2	18	17	27	25
3	9	8	16	15
4	72	67	20	19
Σ	107	100	107	100

data in Table 2. The annular electron diffraction patterns of the first type occur five times more frequently in the C regions of the composite. Contrariwise, electron diffraction patterns of the fourth type, which are characteristic of coarse crystals, are found 3.5 times more frequently in the bulk of the composite. The aforesaid suggests that the carbon region C is a volume into which the Si–Al melt did not penetrate and its structure and composition remained similar to those of the starting carbon material. The increase in the share of the coarsely crystalline component in the carbon remaining in the bulk of the composite (Table 2) is presumably due to the following: the finely crystalline component of the graphite phase is the first to be involved in carbide formation.

Part of discrete electron diffraction patterns obtained from the bulk of the composite is attributed to silicon carbide and silicon with a coherent domain size of more than 50 μm. The appearance of the electron diffraction patterns of silicon is virtually the same over the entire cross section of the samples. The interplanar spacings calculated from these diffraction patterns are in good agreement with the ASTM file. Direct measurements of the coherent domains with the use of dark-field images obtained using the reflection 111 demonstrated that they are 70 nm and more in size. The interplanar spacings of silicon exceed by approximately 0.001 nm those from the ASTM file, which indicates the existence of solid solutions of aluminum in silicon. Deviations from the interplanar spacing listed in the ASTM file are observed in the vicinity of the C regions. This may be due to an increase in the concentration of the aluminum impurity. The size of the coherent domain in silicon, measured using the dark-field images obtained with the reflection 110, varies within the range 50–400 nm.

Characteristically, the electron diffraction patterns of aluminum are constituted by nearly solid rings and can only be recorded at the interface between the bulk of the composite and the C regions. The sizes of aluminum crystals, measured from the light-field image, are 8–12 nm.

The X-ray diffraction patterns obtained from the bulk of the PG–AS, GP–0.5AS, and MG–AS composites (Fig. 3, light hatching) show reflections characteristic of β-SiC, turbostratic carbon, and silicon. The intensities of reflections from different phases in the composites (peak heights) are listed in Table 3. It can be seen that the lowest intensity of the diffraction reflections of β-SiC, which is contained in the composites, is observed for PG–AS. For the other two of the materials studied (GP–0.5AS and MG–AS), the intensities of the diffraction peaks of β-SiC are by a factor of approximately 1.3 higher. This indicates that the amount of silicon carbide grows as the density of the starting carbon supports and the concentration of aluminum in the melt become higher (Tables 1, 3).

Table 3 shows that the intensity of carbon lines increases, on the average, by a factor of 1.4 and 2 for GP–0.5AS and MG–AS, respectively, as compared to the PG–AS composite. Such a change in the intensities indicates that the amount of residual carbon, which has not reacted with the silicon melt, becomes greater. The possible reason is the same: the increased density of the carbon materials and higher concentration of aluminum (Tables 1, 3).

The relative intensities of the silicon reflections

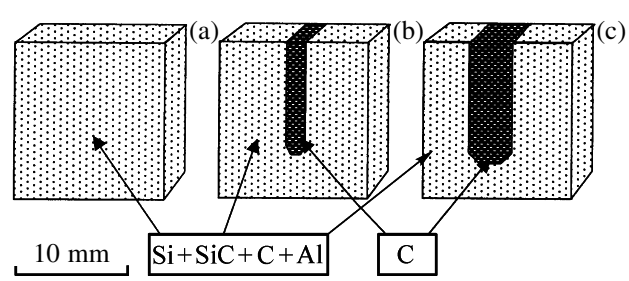

Fig. 3. Schematic of edge surfaces of C–SiC–Si–Al composites: (a) PG–AS, (b) GP–0.5AS, and (c) MG–AS.

Table 3. Structural characteristics of the main phases of C–SiC–Si–Al composites, determined from the profiles of reflections with 100% intensity, and the intensities of reflections from the main phases in the X-ray diffraction patterns of the composites, measured under the identical conditions

Composite			PG–AS		GP–0.5AS		MG–AS	
SiC d_{111}, nm L_{111}, nm I_{111}, rel. units			 0.2518 230 1677		 0.2518 260 2079		 0.2518 (0.2521*) 220 (140*) 2053 (194*)	
ASTM SiC								
d, Å	*I*, %	*hkl*	*I*, rel. units	*I*, %	*I*, rel. units	*I*, %	*I*, rel. units	*I*, %
2.51	100	111	158	100	200	100	201	100
2.18	20	200	20	12.7	30	15	28	14
1.54	63	220	45	28.5	75	37.5	66	32.8
1.31	50	311	38	24	48	24	52	25.8
1.26	5	222	8	5	11	5.5	10	5
Σ			269	100	368	135	357	132
C: d_{002}, nm L_{002}, nm I_{002}, rel. units			 0.3371 38.1 377		 0.3387 33.5 713		 0.3373 (0.3388**) 37.7 (333.5**) 876 (9117**)	
ASTM C								
3.348	100	002	65	100	99	100	141	100
2.127	3	100	3	4.6	3	3	6	4.3
2.027	15	101	5	4.6	4	4	6	3.5
1.647	6	004	3	4.6	2	2	5	3.5
1.228	4	110	5	7.7	3	3	8	5.6
Σ			81	100	111	137	166	205
Si: d_{111}, nm L_{111}, nm I_{111}, rel. units			 0.3147 230 1156		 0.3146 >500 836		 0.3145 (0.3153*) >500 (420*) 416 (227*)	
ASTM Si								
3.1355	100	111	250	100	22	100	30	100
1.9201	55	220	47	18.8	4	18.2	21	70
1.6375	30	311	38	15.2	6	27.3	9	30
1.3577	6	400	18	7.2	–	–	–	–
1.2459	11	331	5	2	–	–	3	10
Σ			358	1118	32	100	63	193

* Boundary of the carbon region C.
** Carbon region C.

Table 4. Variation of the relative intensity of the strongest reflections from the main phases across a sample of the MG–AS composite

Measurement point	l, nm	C(002)			Si(111)		SiC(111)	
		I, rel. units	L, nm	d, nm	I, rel. units	d, nm	I, rel. units	d, nm
1	0.00	23	37.7	0.3376	3.5	0.3145	30	0.2518
2	3.60	139	35.4	0.3384	2.5	0.3153	12	0.2521
3	6.65	229	33.5	0.3388	0	–	0	–
4	9.10	221	33.9	0.3388	0	–	1	–
5	11.05	48	34.6	0.3386	4	0.3153	25	0.2520
6	12.45	32	36.4	0.3382	9	0.3149	30	0.2519
7	14.25	31	37.6	0.3376	5.5	0.3145	28	0.2518

are in disagreement with those in the ASTM files (Table 3). In addition, a minor rotation (by ~5°) of the section of a composite leads to a strong (severalfold) change in the intensities of the diffraction peaks of Si. This indicates that the silicon crystals formed in the composites are textured, which hinders a correct comparative analysis. However, judging from the total intensity Σ of all the reflections, it can be stated that the highest concentration of Si is observed in the PG–AS composite (Σ_{PG-AS} exceeds by a factor of approximately 11 the total intensity of the Si lines in the GP–0.5AS composite).

The structural characteristics of the main phases (β-SiC, C, and Si) were determined by analyzing the profiles of the strongest reflections from these phases (Table 3). It was established that the interplanar spacings d_{002} of the carbon phase are in the range 0.3371–0.3377 nm, and the average sizes of the coherent domain, 30.2–37.7 nm. The differences are presumably due to the different structures of the starting carbon materials. Strong differences are observed between the characteristics of crystalline carbon in the bulk of the MG–AS composite and in the carbon region C (Table 4). Table 4 shows that the interplanar spacings and the integral intensity in the C region are larger, and the average size of the coherent domains smaller, than those in the bulk of the composite. In all probability, the finely crystalline component of the carbon material has the highest reactivity and is the first to enter into the reaction with silicon to form a carbide. Noteworthy is one more specific feature of crystal formation: the coherent domains of silicon carbide at the boundary of the C region are smaller than in the bulk of the composite (Table 3). This is due to the fact that β-SiC is formed in the boundary region under the conditions of silicon deficiency.

The interplanar spacings d_{111} of silicon in the composites are 0.3145–0.3153 nm, which exceeds the tabulated value (0.3135 nm) and points to the formation of solid solutions of aluminum in silicon. The average size of the coherent domains exceeds 200 nm.

To elucidate the mechanism of formation of those regions of the composites into which the silicon melt does not penetrate, the variation of the phase composition across a sample of a composite was studied in accordance with the scheme in Fig. 1. The results obtained are listed in Table 4 and shown in Fig. 4. It was established that the content of silicon carbide and silicon in the carbon region C of the composite is

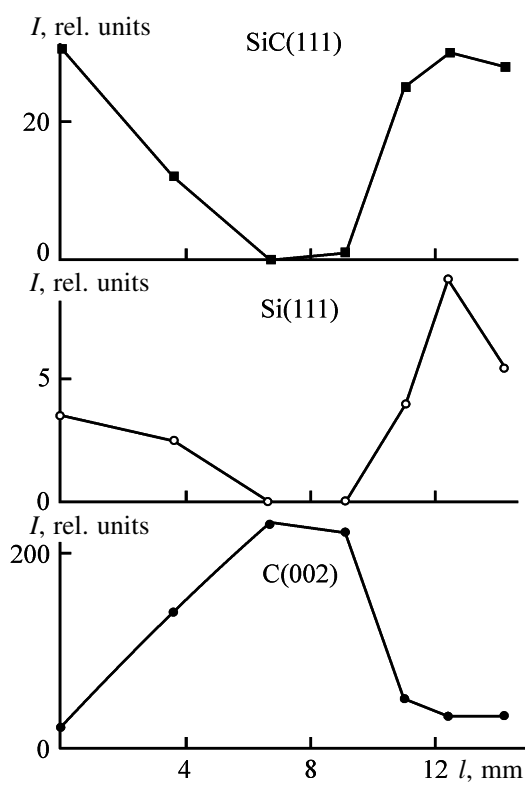

Fig. 4. Variation of the intensity I of the reflections 111 for silicon carbide, 111 for silicon, and 002 for carbon across a sample of the MG–AS composite.

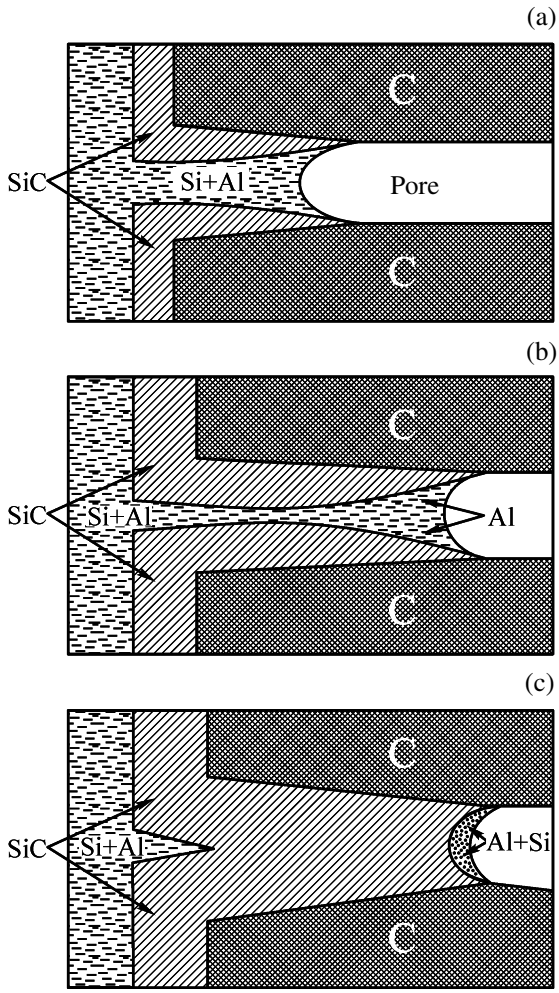

Fig. 5. Mechanism of formation of carbon regions in C–SiC–Si–Al composites: (a) Motion of the Si–Al melt along a pore at the beginning of the process, (b) overgrowth of the pore, and (c) formation of an SiC layer beyond the overgrowth point through spreading of the remaining part of the melt that penetrated into the pore.

virtually zero and their content in the bulk of the composite decreases toward the boundary of the purely carbon region. Contrariwise, the intensity of the line 002 of carbon increases and reaches its maximum value in the C region.

The results obtained suggest the following formation mechanism of the structure of the four-component composite C–SiC–Si–Al. The composites are formed by reaction with the Si–Al melt, which spreads along the capillaries (pores) of the starting carbon supports. Since silicon is constantly spent in the process for SiC formation, the concentration of the impurity (aluminum) at the melt motion front must increase, as it occurs when C–SiC–Si–Cu is formed [4]. This is confirmed by the experimentally observed dependence of the interplanar spacings d_{111} of metallic silicon present in the composite on the cut depth (Table 4). The average interplanar spacing d_{111} varies from 0.3145 to 0.3153 nm and exceeds that for pure silicon (0.3135 nm). The hypothesis is also confirmed by the formation of aluminum crystals at the boundary of the carbon region C. The concentration of aluminum in silicon on the surface of the MG–AS composite, evaluated using Vegard's law [6], is two times smaller than that at the boundary of the volume of the composite in which the reaction with the Si–Al melt did not occur. The increase in the concentration of aluminum at the front of the melt moving along the capillaries must lead to a proportional acceleration of the crystallization of SiC. The catalytic effect of aluminum on the growth rate of SiC is confirmed by the results of comparative studies of carbide formation in Si, Si–Al, and Si– Cu melts brought in contact with a carbon surface in the initial stage (2 to 120 s) of the process, reported in [7].

The motion of the front of the Si–Al melt is illustrated by the scheme in Fig. 5. The amount of SiC formed at the beginning of the interaction between the silicon melt and carbon gradually increases, so that at a small diameter of the pores they must be overgrown with a layer of rapidly formed SiC. As a result, further supply of the melt along the capillaries is terminated (Fig. 5b). Regions into which no melt has penetrated are formed in the composite. A part of the unreacted melt, which is beyond the clogging point, gradually flows toward the defective region (Fig. 5c), with the result that the boundary of this region becomes less abrupt and the amount of SiC formed gradually varies in going from the surface of the composite to the C region. This mechanism of formation of structural heterogeneities differs from that for the case of four-component composites and copper, in which the melt motion terminates as a result of an increase in the contact angle [4]. Strongly different effects of Cu and Al on the phase boundaries of other semiconductors have also been reported [8].

The acceleration of carbide formation at the interface between the Si–Al melt and carbon, compared to that for a system with no aluminum additives, is presumably due to a higher rate of carbon dissolution in the melt at the beginning of the interaction between the melt and the carbon surface. After an SiC layer is formed on the carbon surface, the rate of carbide formation is limited by diffusion of carbon across the carbide layer and the impurities present in the melt cannot affect the process to any noticeable extent. However, at the beginning of the interaction, when the SiC layer is not formed yet, the surface tension at the

melt–carbon phase boundary decreases to zero, and even becomes negative [9]. This may lead to diffusion of carbon particles into the melt, to form a colloid solution [9]. The thickness of the primary SiC layer formed on the carbon surface must be proportional to the amount of carbon dissolved in the melt at the beginning of the interaction. Therefore, the catalytic effect of aluminum on the formation of a carbide is, in the authors' opinion, due to the fact that its presence in the silicon melt leads to dissolution of a greater amount of carbon at the beginning of the interaction between the melt and the carbon surface.

CONCLUSION

Spatially heterogeneous regions are formed in C–SiC–Si–Al composites as a result of a catalytic action of aluminum on the process of carbide formation. The formation of regions into which no melt penetrates can be precluded by lowering the concentration of aluminum in the silicon melt and making larger the capillaries (pores) in the starting carbon support.

REFERENCES

1. Tarabanov, A.S. and Kostikov, V.I., *Silitsirovannyi grafit* (Siliconized Graphite), Moscow: Metallurgiya, 1977.
2. Gnesin, G.G., *Karbidokremnievye materialy* (Silicon Carbide Materials), Moscow: Metallurgiya, 1977.
3. Virgil'ev, Yu.S., *Izv. Ross. Akad. Nauk, Neorg. Mater.*, 1997, vol. 33, no. 6, pp. 683–690.
4. Belenkov, E.A., Tyumentsev, V.A., Koshelev, Yu.I., and Sheinkman, A.I., *Izv. Ross. Akad. Nauk, Neorg. Mater.*, 1992, vol. 28, no. 10/11, pp. 2096–2099.
5. Nagornyi, V.G., Kotosonov, A.S., Ostrovskii, V.S., *et al.*, *Svoistva konstruktsionnykh materialov* (Properties of Structural Materials), Moscow: Metallurgiya, 1975.
6. Umanskii, Ya.S., Skakov, Yu.A., Ivanov, A.N., and Rastorguev, L.N., *Kristallografiya, rentgenografiya i elektronnaya mikroskopiya* (Crystallography, X-ray Diffraction Analysis, and Electron Microscopy), Moscow: Metallurgiya, 1982.
7. Belenkov, E.A., Tyumentsev, V.A., and Fotiev, A.A., *Izv. Ross. Akad. Nauk, Neorg. Mater.*, 1997, vol. 33, no. 3, pp. 324–328.
8. Bechstedt, F. and Enderlein, R., *Semiconductor Surface and Interface: Their Atomic and Electronic Structure*, Berlin: Akademie, 1988.
9. Elyutin, V.P., Kostikov, V.I., Maurakh, M.A., *et al.*, *Konstruktsionnye materialy na osnove ugleroda* (Carbon-Based Structural Materials), Moscow: Metallurgiya, 1974, vol. 9, pp. 190–200.